

Article

Metastable Kitaev Magnets

Faranak Bahrami ¹, Mykola Abramchuk ¹, Oleg Lebedev ² and Fazel Tafti ^{1,*}

¹ Department of Physics, Boston College, Chestnut Hill, MA 02467, USA; bahrami@bc.edu (F.B.); abramchukns@gmail.com (M.A.)

² Laboratoire CRISMAT, ENSICAEN-CNRS UMR6508, 14050 Caen, France; oleg.lebedev@ensicaen.fr

* Correspondence: fazel.tafti@bc.edu

Abstract: Nearly two decades ago, Alexei Kitaev proposed a model for spin-1/2 particles with bond-directional interactions on a two-dimensional honeycomb lattice which had the potential to host a quantum spin-liquid ground state. This work initiated numerous investigations to design and synthesize materials that would physically realize the Kitaev Hamiltonian. The first generation of such materials, such as Na₂IrO₃, α-Li₂IrO₃, and α-RuCl₃, revealed the presence of non-Kitaev interactions such as the Heisenberg and off-diagonal exchange. Both physical pressure and chemical doping were used to tune the relative strength of the Kitaev and competing interactions; however, little progress was made towards achieving a purely Kitaev system. Here, we review the recent breakthrough in modifying Kitaev magnets via topochemical methods that has led to the second generation of Kitaev materials. We show how structural modifications due to the topotactic exchange reactions can alter the magnetic interactions in favor of a quantum spin-liquid phase.

Keywords: metastable; magnetism; topochemical



Citation: Bahrami, F.; Abramchuk, M.; Lebedev, O.; Tafti, F. Metastable Kitaev Magnets. *Molecules* **2022**, *27*, 871. <https://doi.org/10.3390/molecules27030871>

Academic Editor: Paul A. Maggard

Received: 21 December 2021

Accepted: 24 Januar 2021

Published: 27 Januar 2021

Publisher's Note: MDPI stays neutral with regard to jurisdictional claims in published maps and institutional affiliations.



Copyright: © 2022 by the authors. Licensee MDPI, Basel, Switzerland. This article is an open access article distributed under the terms and conditions of the Creative Commons Attribution (CC BY) license (<https://creativecommons.org/licenses/by/4.0/>).

1. Introduction

Recently, 4d/5d honeycomb layered materials have been vigorously studied due to their potential in realizing a quantum spin-liquid (QSL) ground state [1–8]. First introduced by Alexei Kitaev in 2006, the Kitaev model is an exactly solvable theoretical model with bond-dependent Ising interactions among spin-1/2 degrees of freedom on a two-dimensional (2D) honeycomb lattice, which is described by the Kitaev Hamiltonian: $\mathcal{H} = -\sum K_{\gamma} S_i^{\gamma} S_j^{\gamma}$ [9]. The ground state of this system is magnetically frustrated and is predicted to be a QSL [9]. The applications of a Kitaev QSL in quantum information and the possibility of realizing Majorana fermions have inspired numerous investigations into quasi-2D honeycomb materials [1,3,10–12]. Such materials are colloquially labelled Kitaev magnets as they support a sizable Kitaev interaction; however, one needs to consider that other interactions such as Heisenberg exchange are also present and compete with the Kitaev interaction in the so-called Kitaev magnets [3,10].

The first generation of Kitaev magnets, namely Na₂IrO₃, α-Li₂IrO₃, Li₂RhO₃, and α-RuCl₃, were synthesized using conventional solid-state methods at high temperatures ($T > 700$ °C). In these materials, heavy transition metal ions (Ru³⁺, Rh⁴⁺, and Ir⁴⁺) are octahedrally coordinated with oxygen or chlorine atoms (Figure 1a), and the edge-sharing octahedra create honeycomb layers (Figure 1b). The combination of octahedral crystal electric field (CEF) and strong spin-orbit coupling (SOC) splits the five-fold degenerate *d*-levels and leaves one electron in the isospin-1/2 ($J_{\text{eff}} = 1/2$) state necessary for the Kitaev model (Figure 1c) [1,4,7,9,13].

Finding new Kitaev magnets, beyond the first-generation compounds, has become a frontier challenge in solid-state chemistry. Prior attempts to replace Na with K in Na₂IrO₃ or replacing Cl with Br in α-RuCl₃ has led to other stable phases with different structures instead of the honeycomb lattice [14,15]. The amount of physical pressure required to substantially tune the interactions is too high [16] and chemical doping leads to a change

of spin state [17]. Therefore, recent success in synthesizing a second generation of Kitaev magnets where magnetic interactions can be tuned by topochemical methods has revitalized the field. In this review, we will first explain the different types of exchange reactions (partial and complete), then discuss the interplay between topochemical reactions and magnetism, and finally present heat capacity and magnetization data to compare the properties of the first- and second-generation Kitaev magnets.

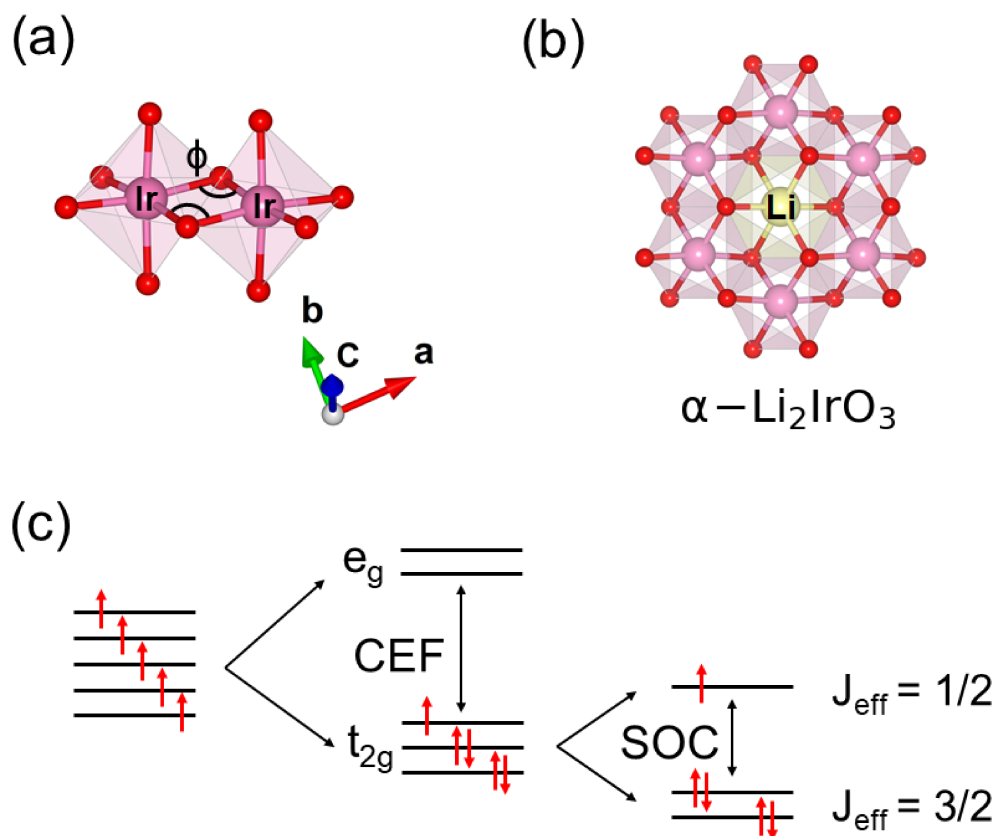
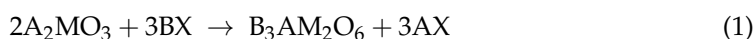


Figure 1. (a) The bond angle (ϕ) between edge-shared octahedral units plays a significant role in tuning the magnetic interactions. (b) Edge-sharing octahedral units create a honeycomb structure in Kitaev magnets such as $\alpha\text{-Li}_2\text{IrO}_3$ and Na_2IrO_3 . (c) Interplay between CEF and SOC creates the isospin-1/2 state in the Kitaev magnets.

2. Topotactic Exchange Reactions

The second-generation Kitaev magnets are metastable compounds, i.e., they have a higher enthalpy of formation and a lower decomposition threshold compared to stable counterparts [18]. Thus, it is impossible to synthesize them with conventional solid-state methods at high temperatures. Instead, they are stabilized through topochemical reactions from the first-generation compounds under mild conditions. As shown schematically in Figure 2 the global symmetries of the unit cell do not change during a topochemical reaction. However, the local parameters such as bond lengths and bond angles are modified efficiently.

Topotactic exchange reactions can be either partial (Figure 2a) or complete (Figure 2b). The most general formulation of a partial exchange reaction is



where the interlayer A-atoms (typically Li or Na) in a stable honeycomb structure A_2MO_3 are exchanged with the B-atoms (typically Cu, Ag, and H) from a halide, nitrate, or sulfate compound BX. For example, Figure 2a corresponds to $\text{A} = \text{Li}$, $\text{B} = \text{Ag}$, $\text{M} = \text{Ir}$, and $\text{X} = \text{NO}_3$ for the synthesis of $\text{Ag}_3\text{LiIr}_2\text{O}_6$ from $\alpha\text{-Li}_2\text{IrO}_3$. Replacing the interlayer Li atoms by H,

Cu, or Ag, in α -Li₂IrO₃ has recently produced H₃LiIr₂O₆, Cu₃LiIr₂O₆, and Ag₃LiIr₂O₆, respectively [19–23].

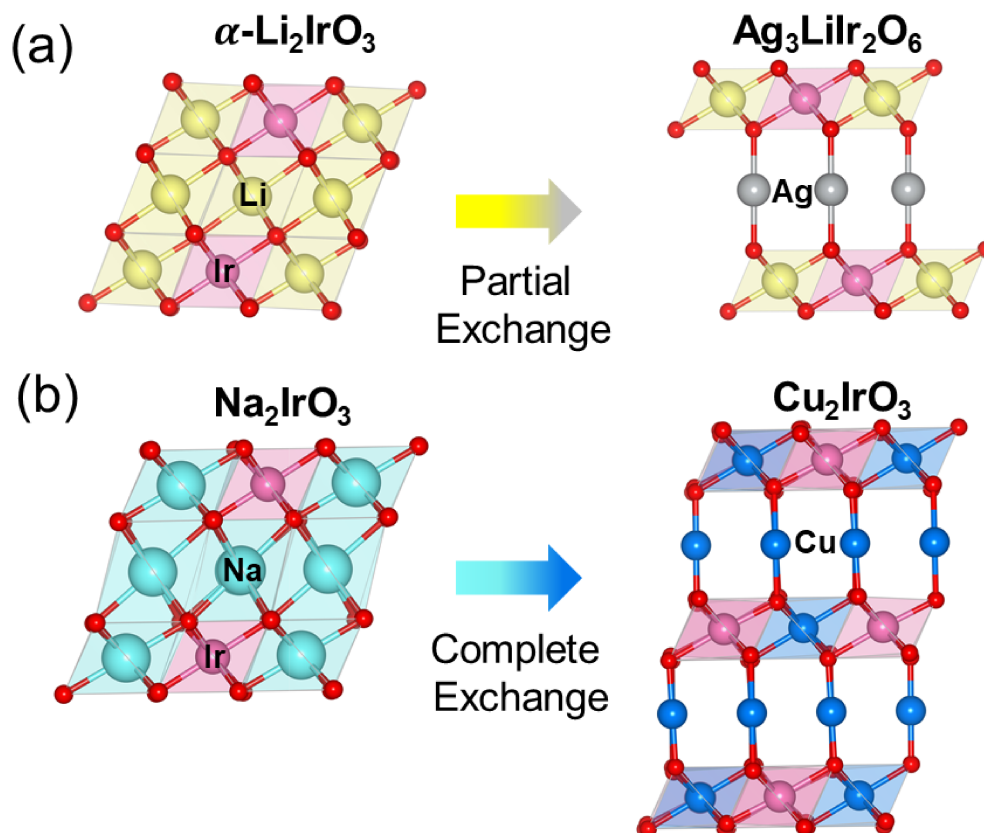


Figure 2. Synthesis of the second-generation Kitaev magnets from the first-generation materials through (a) partial and (b) complete exchange reactions. Both generations have honeycomb layers. The topochemical change of interlayer coordination from octahedral to linear modifies the intra-layer Ir-O-Ir bond angles due to the change of oxygen positions.

In a complete topotactic exchange reaction, all A-atoms within and between the layers are replaced by the B-atoms.



For example, Figure 2b corresponds to A = Na, B = Cu, M = Ir, and X = Cl for the synthesis of Cu₂IrO₃ from Na₂IrO₃. A complete exchange reaction is much less likely to happen and so far, Cu₂IrO₃ is the only known system in this category [24]. It is noteworthy that the copper atoms in Cu₂IrO₃ are not entirely in a Cu⁺ state. Both X-ray absorption and electron energy loss spectroscopy (XAS and EELS) confirmed a mixed valence of Cu⁺/Cu²⁺ = 1/1 within the honeycomb layers [25]. A mixed valence of copper induces a mixed valence of iridium (Ir⁺³/Ir⁺⁴) and leads to magnetic disorder and spin-glass behavior [25,26].

Topochemical reactions enable us to considerably change the coordination environment, bond lengths, and bond angles between the first- and second-generation compounds (Figure 2). In a partial exchange reaction, the octahedrally coordinated interlayer alkaline atoms (A) in the parent compounds such as A₂BO₃ are replaced by B = H, Cu, or Ag atoms with a linear (dumbbell) coordination in the second-generation compound B₃AM₂O₆ (Figure 2a). This change in the interlayer chemical bond coordination increases the interlayer spacing when B = Cu or Ag, and decreases it when B = H. It also changes the position of O atoms in the honeycomb layers of the product (second-generation) compounds and thus changes the bond angles and bond lengths that determine the magnetic interactions.

In a complete exchange reaction (Figure 2b), not only are the interlayer alkaline atoms (A) and their associated chemical bonds changed, but the alkaline cations within the honeycomb layers are also replaced by the B-atoms. The increasing of the interlayer spacing and weakening of interlayer chemical bonds are still valid in a complete exchange reaction.

3. Synthesis Details

The first-generation Kitaev magnets are prepared via conventional solid-state reaction at high temperatures ($T \geq 700$ K) in air, under vacuum, or under the flow of oxygen/argon gas [7,13,27]. To improve the sample quality and remove stacking faults, it is necessary to perform successive stages of grinding and heating. For example, the X-ray patterns in Figure 3a show that the quality of α - Li_2IrO_3 samples improve by repeating the heat cycles. Specifically, the superstructure peaks between 20 and 30 degrees (inset of Figure 3a) that represent the honeycomb ordering become more pronounced in each iteration. Typically, improving the quality of the first-generation compound will improve the quality of the second-generation material after the exchange reaction [28].

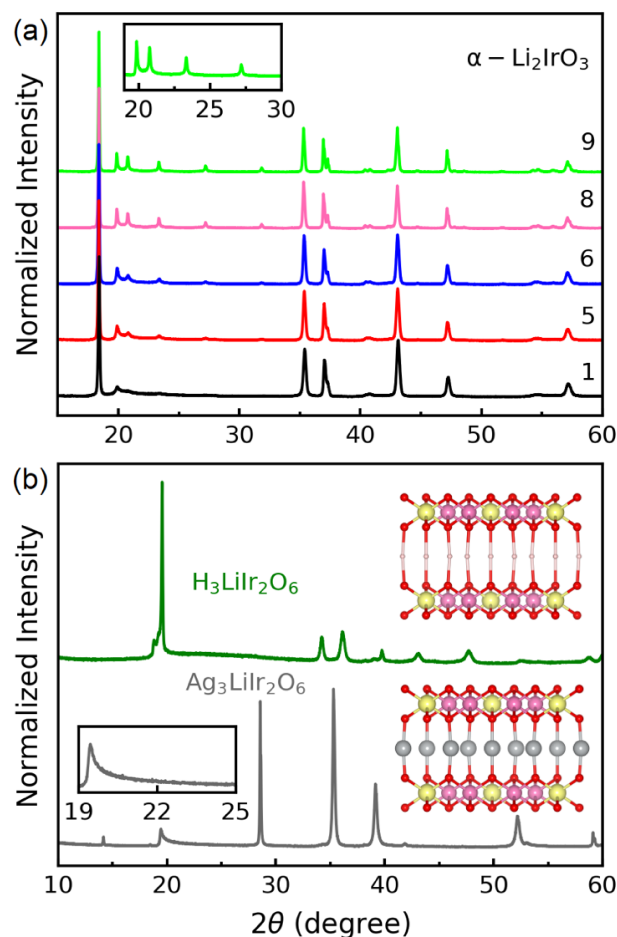
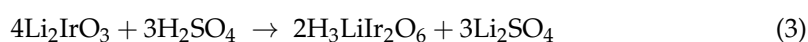


Figure 3. (a) After each heat cycle, the powder X-ray pattern of α - Li_2IrO_3 shows more pronounced peaks, especially between 20 and 30 degrees where the honeycomb Bragg peaks appear. The number of times each sample has been reheated is shown on the right above its respective pattern. (b) The X-ray patterns of two second-generation Kitaev magnets, $\text{H}_3\text{LiIr}_2\text{O}_6$ (green) and $\text{Ag}_3\text{LiIr}_2\text{O}_6$ (gray data, reproduced from [28]). The inset shows the asymmetric broadening of the honeycomb Bragg peaks in $\text{Ag}_3\text{LiIr}_2\text{O}_6$ due to stacking faults. In $\text{H}_3\text{LiIr}_2\text{O}_6$, the honeycomb peaks are hardly discernible due to high structural disorder.

The topotactic cation exchange reaction must be conducted at low temperatures ($T \leq 400$ K) [24,28,29], since higher temperatures will decompose the metastable product.

The second-generation Kitaev magnets are prepared by modifying the interlayer atoms and the associated chemical bonds, and therefore they have more stacking faults than their parent compounds [28,30]. This can be seen in the inset of Figure 3b that shows an asymmetric broadening of the honeycomb Bragg peaks in $\text{Ag}_3\text{LiIr}_2\text{O}_6$. Unlike solid-state reactions, topotactic exchange cannot be repeated to improve the sample quality. Thus, removing the stacking faults in these materials remains an open challenge.

Details of the synthesis procedures for Cu_2IrO_3 and $\text{Ag}_3\text{LiIr}_2\text{O}_6$ have been published by Abramchuk and Bahrami et al. previously [19,24,28]. Here, we present more details about the synthesis of $\text{H}_3\text{LiIr}_2\text{O}_6$ based on the earlier work of Bette et al. [31]. Polycrystalline samples of $\text{H}_3\text{LiIr}_2\text{O}_6$ are synthesized using a modified version of Equation (1).



After synthesizing a high-quality sample of $\alpha\text{-Li}_2\text{IrO}_3$ (Figure 3a), approximately 300 mg of the material was added to a 10 mL Teflon-lined steel autoclave filled with H_2SO_4 acid (1 M solution) and heated to 120 °C for several days. After completing the reaction, the product was washed with water and the quality was verified using X-ray diffraction (Figure 3b).

4. Stacking Faults

A comparison between the insets of Figure 3a,b suggests fewer stacking faults in $\alpha\text{-Li}_2\text{IrO}_3$ (sharp and well-separated Bragg peaks from the honeycomb layers) and considerable stacking faults in $\text{Ag}_3\text{LiIr}_2\text{O}_6$ (broadened peaks). The asymmetric broadening of honeycomb peaks is known as the Warren line shape, which is a signature of stacking disorder [32]. The higher amount of stacking faults in the second-generation Kitaev magnets is due to the interlayer chemistry. As shown in Figure 2, each interlayer Li atom in $\alpha\text{-Li}_2\text{IrO}_3$ is octahedrally coordinated with three oxygen atoms from the top and three from the bottom honeycomb layers. In contrast, each Ag atom in $\text{Ag}_3\text{LiIr}_2\text{O}_6$ is connected to only one O atom from the top and one from the bottom layer in a dumbbell (linear) coordination. The weak dumbbell bonds are responsible for the larger interlayer separation in $\text{Ag}_3\text{LiIr}_2\text{O}_6$ and the presence of more stacking faults compared to $\alpha\text{-Li}_2\text{IrO}_3$ [33].

Direct lattice imaging with transmission electron microscopy (TEM) is a powerful tool to study the stacking faults. Figure 4a,b (reproduced from Ref. [28]) are high angle annular dark-field TEM (HAADF-TEM) images of $\alpha\text{-Li}_2\text{IrO}_3$ and $\text{Ag}_3\text{LiIr}_2\text{O}_6$ samples, respectively. Although the stacking sequence in $\alpha\text{-Li}_2\text{IrO}_3$ can be flawless for up to 50 unit cells, $\text{Ag}_3\text{LiIr}_2\text{O}_6$ shows a maximum of 5 unit cells stacked without faults (in the form of twisting between the layers). In $\text{H}_3\text{LiIr}_2\text{O}_6$, the small size of H atoms and their high mobility make the chemical bonds even weaker than in $\text{Ag}_3\text{LiIr}_2\text{O}_6$. As such, $\text{H}_3\text{LiIr}_2\text{O}_6$ has the highest degree of stacking faults among the second-generation Kitaev magnets [29–31]. Therefore, the honeycomb peaks of $\text{H}_3\text{LiIr}_2\text{O}_6$ are not resolved by X-rays (Figure 3b).

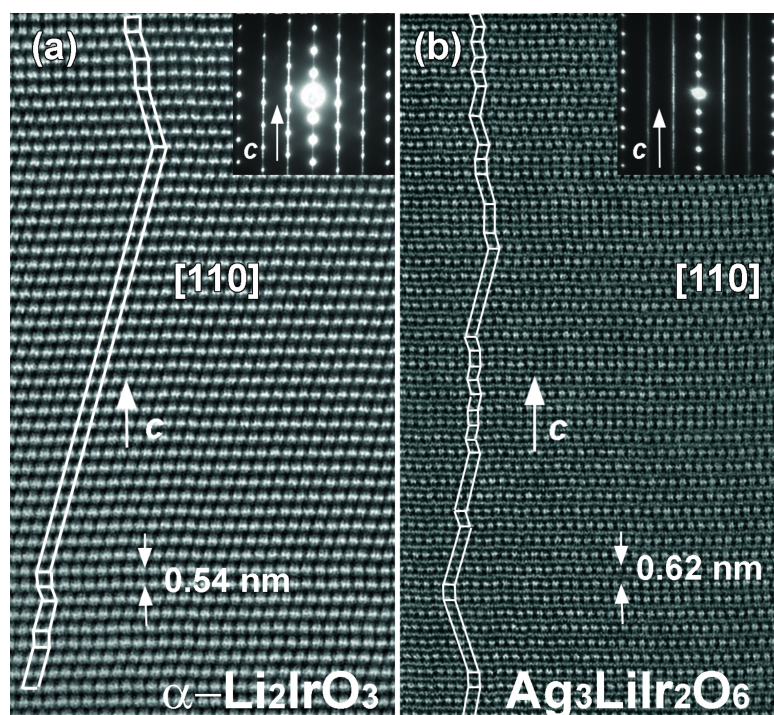


Figure 4. HAADF-TEM images from (a) α - Li_2IrO_3 and (b) $\text{Ag}_3\text{LiIr}_2\text{O}_6$. The images show an abundance of stacking faults in $\text{Ag}_3\text{LiIr}_2\text{O}_6$ unlike α - Li_2IrO_3 , due to the weaker interlayer bonding in the former. The electron diffraction patterns are presented as insets and reveal less streaking in α - Li_2IrO_3 due to fewer stacking faults compared to $\text{Ag}_3\text{LiIr}_2\text{O}_6$.

5. Tuning Magnetic Interactions with Topochemical Methods

As shown in Figure 2, the monoclinic unit cell and the honeycomb ordering in the 2D layers remain unchanged before and after exchange reactions. However, the change of interlayer coordination from octahedral to dumbbell modifies the M-O-M bond angles within the honeycomb layers (Figures 1a and 2). Superexchange magnetic interactions are sensitive to a change of bond angles and thus, topochemical reactions can be used to tune the magnetic interactions. There are at least three terms in the magnetic Hamiltonian of the Kitaev materials.

$$\mathcal{H} = \sum_{\langle i,j \rangle \in \alpha\beta(\gamma)} \left[-K_\gamma S_i^\gamma S_j^\gamma + J \mathbf{S}_i \cdot \mathbf{S}_j + \Gamma (S_i^\alpha S_j^\beta + S_i^\beta S_j^\alpha) \right] \quad (4)$$

The Kitaev term (K) favors QSL, the Heisenberg term (J) favors antiferromagnetic (AFM) ordering, and the off-diagonal exchange term (Γ) controls details of the ordered structure. All three terms can be modified via topochemical reactions as follows.

Figure 5 shows the individual exchange paths for each term in Equation (4). The Kitaev term is an indirect exchange interaction with hopping matrix elements t_{dpd} between the d_{xz} , p_z , and d_{yz} orbitals (Figure 5a) [34,35]. In addition to the indirect exchange (K), Figure 5b shows a direct exchange path for the Heisenberg interaction (J) with hopping matrix element t_{dd} between d_{xy} orbitals, leading to $J \sim t_{dd}^2/U$ in Equation (4) [36]. Finally, a combination of direct and indirect paths in Figure 5c leads to the symmetric off-diagonal exchange, $\Gamma \sim t_{dpd}t_{dd}J_H/U^2$, where J_H is the Hund's coupling between the e_g and t_{2g} orbitals [37,38]. The hopping matrix elements (t_{dd} and t_{dpd}) are tuned by the M-O-M bond angle and the M-M distance which can be tuned by the exchange reactions. For example, (i) the change of oxygen positions within the honeycomb layers due to the change of interlayer coordination in Figure 2 modifies the M-O-M bond angle (ϕ in Figures 1a and 5a) and therefore tunes t_{dpd} ; (ii) according to theoretical calculations [1], the Heisenberg interaction is canceled between the opposite paths if the bond angle ϕ is close to 90° (Figures 1a and 5a);

(iii) the hybridization between the Ag d -orbitals between the layers and O p -orbitals within the layers tunes the ratio of t_{dpa}/t_{dd} .

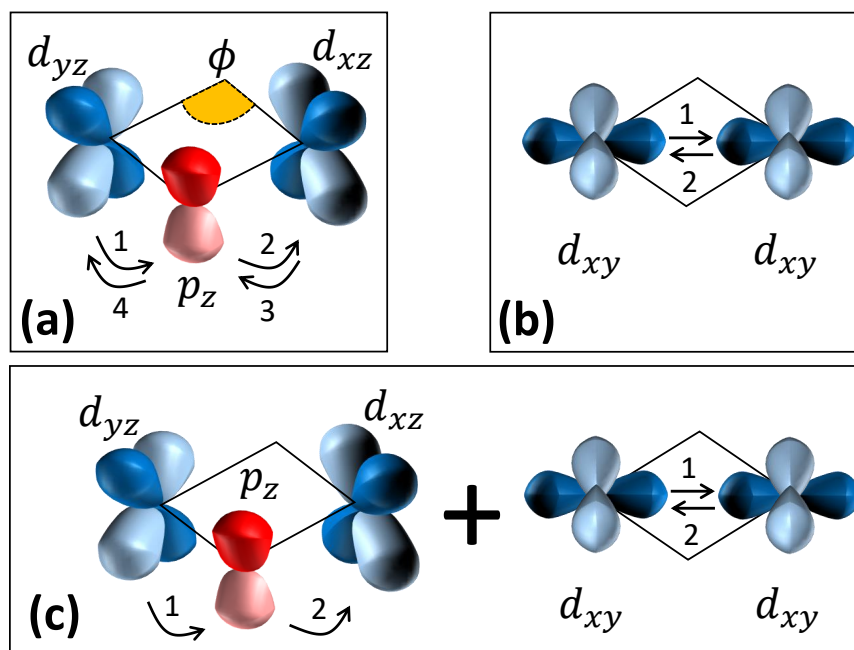


Figure 5. Exchange paths for (a) K , (b) J , and (c) Γ terms in Equation (4). The d and p orbitals are painted in blue and red, respectively. The numbers show the hopping sequence in the perturbation.

6. Magnetic Characterization of Metastable Kitaev Materials

To demonstrate the effect of topochemical modifications on the magnetic interactions (Equation (4) and Figure 5), we compare the heat capacity and magnetic susceptibility of the first- and second-generation Kitaev magnets. The peak in the heat capacity of α - Li_2IrO_3 in Figure 6a confirms long-range magnetic ordering at $T_N = 15$ K. The order has been characterized as an incommensurate spiral by recent neutron scattering and muon spin relaxation (μSR) experiments [5,8]. As shown in Figure 6a, this peak is shifted to lower temperatures in $\text{Ag}_3\text{LiIr}_2\text{O}_6$ and seemingly disappeared in $\text{H}_3\text{LiIr}_2\text{O}_6$. The suppression of T_N in second-generation compounds $\text{Ag}_3\text{LiIr}_2\text{O}_6$ and $\text{H}_3\text{LiIr}_2\text{O}_6$ is a positive sign of approaching the QSL phase, where long-range order is replaced by long-range quantum entanglement [3,10]. A recent μSR experiment [28] has shown a similar incommensurate spiral order in $\text{Ag}_3\text{LiIr}_2\text{O}_6$; however, the long-range order develops at 8 K in $\text{Ag}_3\text{LiIr}_2\text{O}_6$, well below $T_N = 15$ K in α - Li_2IrO_3 . Thus, the topochemical modification of bond angles seems to strengthen K and weaken J in Equation (4). A recent nuclear magnetic resonance (NMR) experiment has shown the absence of long-range order in $\text{H}_3\text{LiIr}_2\text{O}_6$, which is another promising result toward the discovery of a QSL phase [29].

A similar trend is observed in Figure 6b for the first-generation material Na_2IrO_3 that shows a peak at $T_N = 15$ K and its second-generation counterpart Cu_2IrO_3 that does not show a peak but seems to have a broad anomaly below 5 K. Neutron scattering experiments have confirmed a zigzag AFM order in Na_2IrO_3 [39]. Recent μSR and NMR experiments have revealed a coexistence of static and dynamic magnetism below 5 K in Cu_2IrO_3 but without a long-range order, suggesting proximity to the QSL phase [25,40].

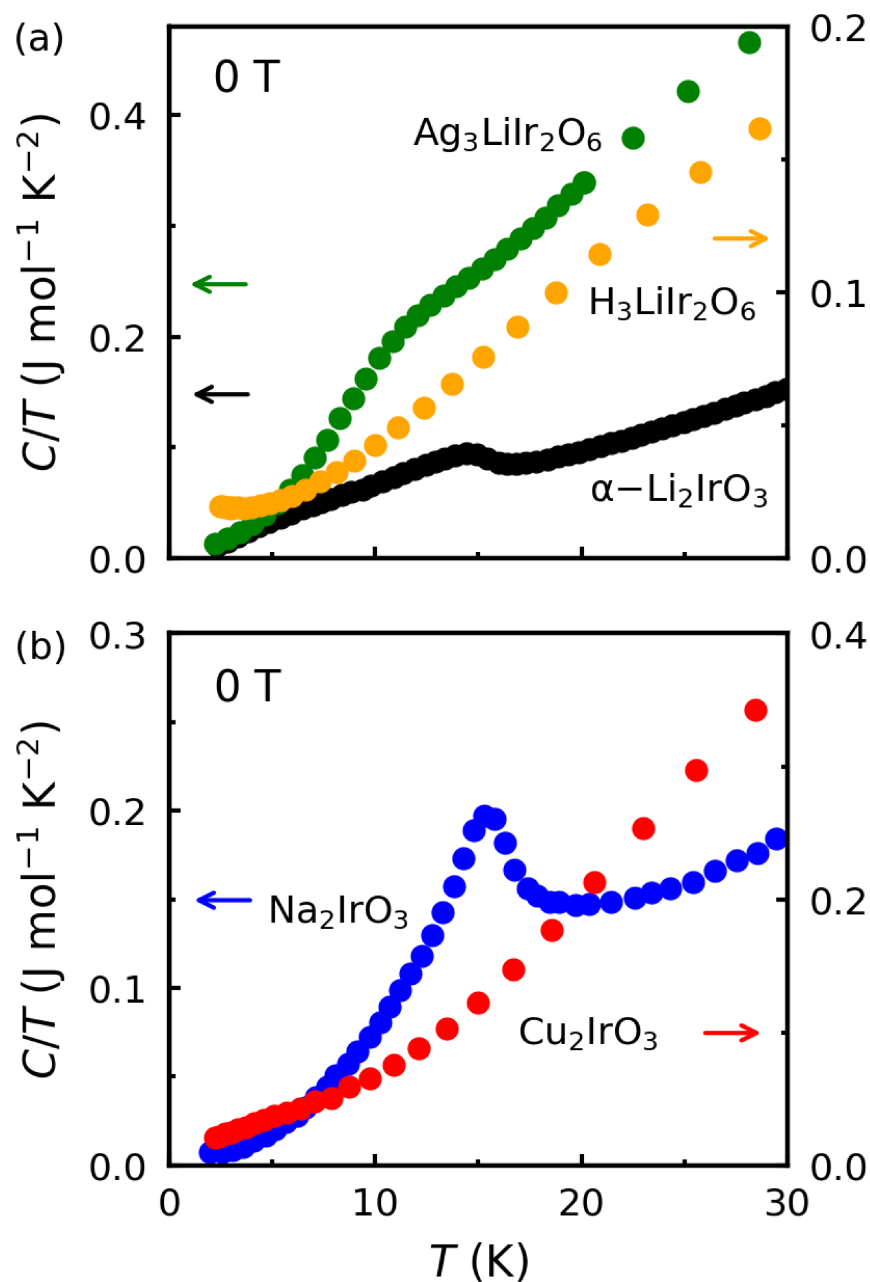


Figure 6. (a) Heat capacity (C/T) plotted as a function of temperature below 30 K for the first-generation Kitaev magnet $\alpha\text{-Li}_2\text{IrO}_3$ and its second-generation derivatives $\text{Ag}_3\text{LiIr}_2\text{O}_6$ and $\text{H}_3\text{LiIr}_2\text{O}_6$. The data for $\alpha\text{-Li}_2\text{IrO}_3$ and $\text{Ag}_3\text{LiIr}_2\text{O}_6$ are reproduced from Refs. [2,28]. (b) A similar comparison is made between Na_2IrO_3 (first generation) and Cu_2IrO_3 (second generation). The data are reproduced from Ref. [24].

The suppression of magnetic ordering due to topochemical changes in metastable Kitaev magnets is also observed in the magnetic susceptibility data. Figure 7a shows the magnetic susceptibility of $\alpha\text{-Li}_2\text{IrO}_3$ (black curve) with a clear anomaly at $T_N = 15$ K indicating the incommensurate spiral AFM order. The green curve representing $\text{Ag}_3\text{LiIr}_2\text{O}_6$ shows two downturns at $T_F = 14$ K and $T_N = 8$ K, corresponding to the onsets of short-range and long-range magnetic orders, respectively [28]. The orange curve representing $\text{H}_3\text{LiIr}_2\text{O}_6$ does not show any evidence of magnetic ordering. Figure 7b shows a similar trend, where the first-generation material Na_2IrO_3 orders at $T_N = 15$ K and the second-generation material Cu_2IrO_3 shows a small peak at 2 K, evidence of short-range spin freezing instead of long-range order.

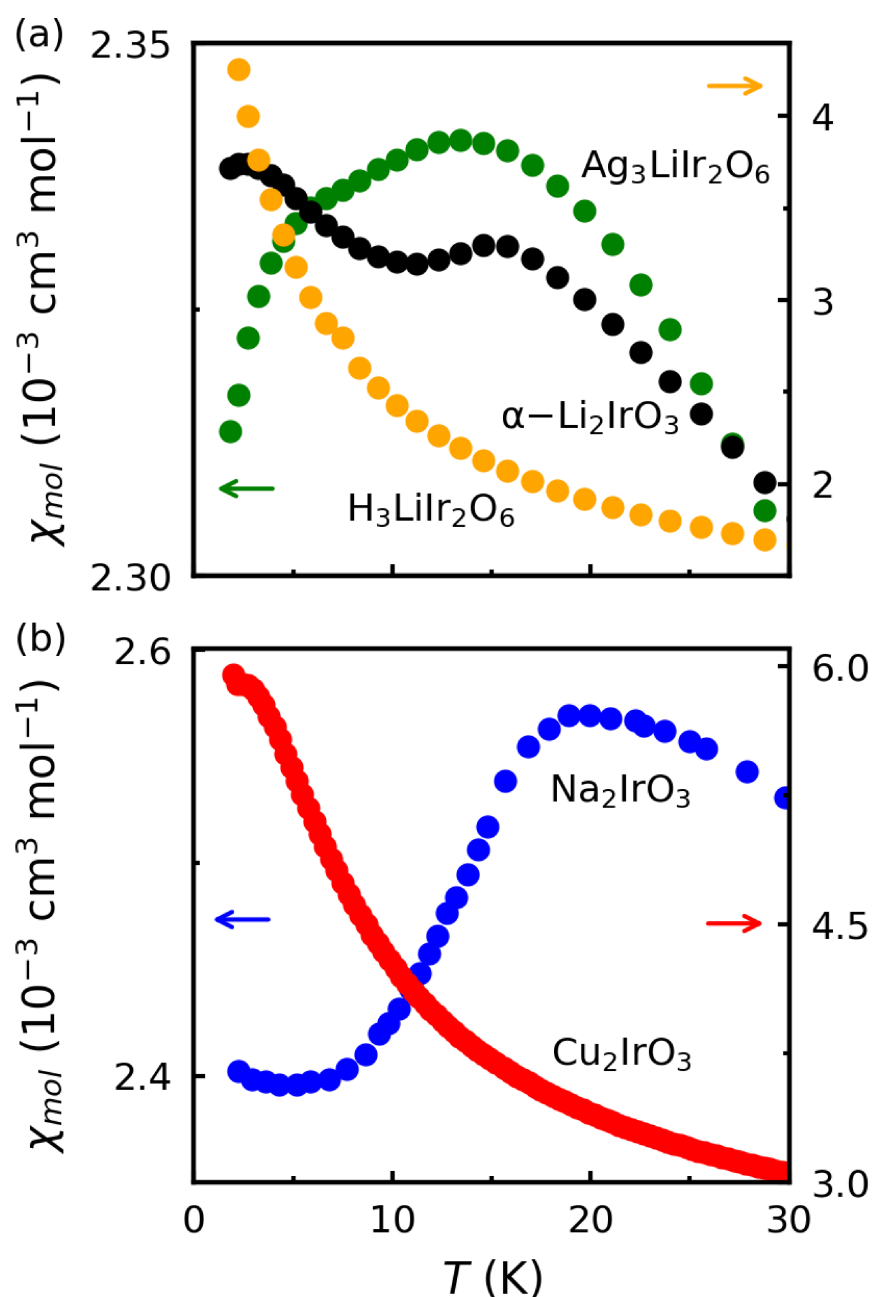


Figure 7. (a) Magnetic susceptibility (χ) plotted as a function of temperature below 30 K for the first-generation Kitaev magnet $\alpha\text{-Li}_2\text{IrO}_3$ and its second-generation derivatives $\text{Ag}_3\text{LiIr}_2\text{O}_6$ and $\text{H}_3\text{LiIr}_2\text{O}_6$. The data for $\alpha\text{-Li}_2\text{IrO}_3$ and $\text{Ag}_3\text{LiIr}_2\text{O}_6$ are reproduced from Refs. [19,28] (The y range for $\alpha\text{-Li}_2\text{IrO}_3$ is from 4.8 to 5.3). (b) A similar comparison is made between Na_2IrO_3 (first generation) and Cu_2IrO_3 (second generation). The data for Na_2IrO_3 and Cu_2IrO_3 are reproduced from Refs. [2,24].

7. Challenges and Opportunities

The above results are exciting; however, they need to be interpreted with caution. Topotactic exchange reactions increase disorder that has adverse effects on magnetism. A recent TEM study has shown that the silver atoms in $\text{Ag}_3\text{LiIr}_2\text{O}_6$ can enter the honeycomb layers and form small inclusions (up to 50 atoms) that disrupt the magnetic ordering [28]. Such a structural disorder can spuriously hide the long-range order and be misinterpreted as evidence of a QSL phase. As noted earlier, $\text{H}_3\text{LiIr}_2\text{O}_6$ is even more disordered compared to $\text{Ag}_3\text{LiIr}_2\text{O}_6$ due to the high mobility of the H atoms, which causes bond randomness and site vacancies within the honeycomb layers [31]. Recent theoretical works show that

the absence of magnetic ordering in $\text{H}_3\text{LiIr}_2\text{O}_6$ may be due to bond randomness and a large number of vacancies [41,42]. Thus, the most important challenge in this field is to optimize the synthesis conditions for a minimum amount of disorder and to find methods of annealing away the stacking faults and vacancies.

One promising approach to minimize the structural disorder in the second-generation Kitaev magnets is to provide single-crystal specimens of this family. Single crystals will also enable accurate determination of the interlayer and intra-layer exchange couplings. Both Raman and nuclear magnetic resonance (NMR) experiments can provide information about the fractionalized (Majorana) excitations in single crystals [23,43].

Metastable Kitaev magnets have opened a new window of opportunity to realizing the quantum spin-liquid ground state. The Majorana excitations of such materials will form the building blocks of a solid-state quantum computer [44]. Braiding algorithms and logical gates have been theoretically developed for such computers [45]. It remains an open challenge for the solid-state chemistry community to synthesize the appropriate materials for such models. Another intriguing opportunity is to find unconventional superconductivity in the Kitaev magnets [46], an exciting theoretical prediction that awaits experimental discovery.

Author Contributions: F.B. and M.A. provided the data and analyses. O.L. provided the TEM images. F.B. and F.T. wrote the paper. All authors have read and agreed to the published version of the manuscript.

Funding: This material is based upon work supported by the Air Force Office of Scientific Research under award number FA2386-21-1-4059.

Institutional Review Board Statement: Not applicable.

Informed Consent Statement: Not applicable.

Data Availability Statement: All data are available from the authors upon request.

Conflicts of Interest: The authors declare no conflict of interest.

References

1. Jackeli, G.; Khaliullin, G. Mott Insulators in the Strong Spin-Orbit Coupling Limit: From Heisenberg to a Quantum Compass and Kitaev Models. *Phys. Rev. Lett.* **2009**, *102*, 017205. [[CrossRef](#)] [[PubMed](#)]
2. Singh, Y.; Manni, S.; Reuther, J.; Berlijn, T.; Thomale, R.; Ku, W.; Trebst, S.; Gegenwart, P. Relevance of the Heisenberg-Kitaev Model for the Honeycomb Lattice Iridates A_2IrO_3 . *Phys. Rev. Lett.* **2012**, *108*, 127203. [[CrossRef](#)] [[PubMed](#)]
3. Takagi, H.; Takayama, T.; Jackeli, G.; Khaliullin, G.; Nagler, S.E. Concept and realization of Kitaev quantum spin liquids. *Nat. Rev. Phys.* **2019**, *1*, 264–280. [[CrossRef](#)]
4. Plumb, K.W.; Clancy, J.P.; Sandilands, L.J.; Shankar, V.V.; Hu, Y.F.; Burch, K.S.; Kee, H.Y.; Kim, Y.J. $\alpha\text{-RuCl}_3$: A spin-orbit assisted Mott insulator on a honeycomb lattice. *Phys. Rev. B* **2014**, *90*, 041112. [[CrossRef](#)]
5. Williams, S.C.; Johnson, R.D.; Freund, F.; Choi, S.; Jesche, A.; Kimchi, I.; Manni, S.; Bombardi, A.; Manuel, P.; Gegenwart, P.; et al. Incommensurate counterrotating magnetic order stabilized by Kitaev interactions in the layered honeycomb $\alpha\text{-Li}_2\text{IrO}_3$. *Phys. Rev. B* **2016**, *93*, 195158. [[CrossRef](#)]
6. Wang, Y.; Osterhoudt, G.B.; Tian, Y.; Lampen-Kelley, P.; Banerjee, A.; Goldstein, T.; Yan, J.; Knolle, J.; Ji, H.; Cava, R.J.; et al. The range of non-Kitaev terms and fractional particles in $\alpha\text{-RuCl}_3$. *NPJ Quantum Mater.* **2020**, *5*, 1–8. [[CrossRef](#)]
7. Todorova, V.; Jansen, M. Synthesis, Structural Characterization and Physical Properties of a New Member of Ternary Lithium Layered Compounds— Li_2RhO_3 . *Z. Anorg. Allg. Chem.* **2011**, *637*, 37–40. [[CrossRef](#)]
8. Choi, S.; Manni, S.; Singleton, J.; Topping, C.V.; Lancaster, T.; Blundell, S.J.; Adroja, D.T.; Zapf, V.; Gegenwart, P.; Coldea, R. Spin dynamics and field-induced magnetic phase transition in the honeycomb Kitaev magnet $\alpha\text{-Li}_2\text{IrO}_3$. *Phys. Rev. B* **2019**, *99*, 054426. [[CrossRef](#)]
9. Kitaev, A. Anyons in an exactly solved model and beyond. *Ann. Phys.* **2006**, *321*, 2–111. [[CrossRef](#)]
10. Knolle, J.; Moessner, R. A Field Guide to Spin Liquids. *Annu. Rev. Condens. Matter Phys.* **2019**, *10*, 451–472. [[CrossRef](#)]
11. Chaloupka, J.; Jackeli, G.; Khaliullin, G. Kitaev-Heisenberg Model on a Honeycomb Lattice: Possible Exotic Phases in Iridium Oxides A_2IrO_3 . *Phys. Rev. Lett.* **2010**, *105*, 027204. [[CrossRef](#)] [[PubMed](#)]
12. Kim, B.J.; Jin, H.; Moon, S.J.; Kim, J.Y.; Park, B.G.; Leem, C.S.; Yu, J.; Noh, T.W.; Kim, C.; Oh, S.J.; et al. Novel $J_{\text{eff}} = 1/2$ Mott State Induced by Relativistic Spin-Orbit Coupling in Sr_2IrO_4 . *Phys. Rev. Lett.* **2008**, *101*, 076402. [[CrossRef](#)]
13. Mehlawat, K.; Thamizhavel, A.; Singh, Y. Heat capacity evidence for proximity to the Kitaev quantum spin liquid in A_2IrO_3 ($\text{A} = \text{Na}, \text{Li}$). *Phys. Rev. B* **2017**, *95*, 144406. [[CrossRef](#)]

14. Weber, D.; Schoop, L.M.; Wurmbrand, D.; Nuss, J.; Seibel, E.M.; Tafti, F.F.; Ji, H.; Cava, R.J.; Dinnebier, R.E.; Lotsch, B.V. Trivalent Iridium Oxides: Layered Triangular Lattice Iridate $K_{0.75}Na_{0.25}IrO_2$ and Oxyhydroxide $IrOOH$. *Chem. Mater.* **2017**, *29*, 8338–8345. [[CrossRef](#)]
15. Merlini, S.; Labella, L.; Marchetti, F.; Toscani, S. Order-disorder transformation in $RuBr_3$ and $MoBr_3$: A two-dimensional Ising model. *Chem. Mater.* **2004**, *16*, 3895–3903. [[CrossRef](#)]
16. Bhattacharjee, S.; Lee, S.S.; Kim, Y.B. Spin—Orbital locking, emergent pseudo-spin and magnetic order in honeycomb lattice iridates. *New J. Phys.* **2012**, *14*, 073015. [[CrossRef](#)]
17. Cao, G.; Schlottmann, P. The challenge of spin—Orbit-tuned ground states in iridates: A key issues review. *Rep. Prog. Phys.* **2018**, *81*, 042502. [[CrossRef](#)]
18. Aykol, M.; Dwaraknath, S.S.; Sun, W.; Persson, K.A. Thermodynamic limit for synthesis of metastable inorganic materials. *Sci. Adv.* **2018**, *4*, eaaq0148. [[CrossRef](#)]
19. Bahrami, F.; Lafargue-Dit-Hauret, W.; Lebedev, O.I.; Movshovich, R.; Yang, H.Y.; Broido, D.; Rocquefelte, X.; Tafti, F. Thermodynamic Evidence of Proximity to a Kitaev Spin Liquid in $Ag_3LiIr_2O_6$. *Phys. Rev. Lett.* **2019**, *123*, 237203. [[CrossRef](#)]
20. Geirhos, K.; Lunkenheimer, P.; Blankenhorn, M.; Claus, R.; Matsumoto, Y.; Kitagawa, K.; Takayama, T.; Takagi, H.; Kézsmárki, I.; Loidl, A. Quantum paraelectricity in the Kitaev quantum spin liquid candidates $H_3LiIr_2O_6$ and $D_3LiIr_2O_6$. *Phys. Rev. B* **2020**, *101*, 184410. [[CrossRef](#)]
21. Roudebush, J.H.; Ross, K.A.; Cava, R.J. Iridium containing honeycomb Delafossites by topotactic cation exchange. *Dalton Trans.* **2016**, *45*, 8783–8789. [[CrossRef](#)] [[PubMed](#)]
22. de la Torre, A.; Zager, B.; Bahrami, F.; DiScala, M.; Chamorro, J.R.; Upton, M.H.; Fabbri, G.; Haskel, D.; Casa, D.; McQueen, T.M.; et al. Enhanced hybridization in the electronic ground state of the intercalated honeycomb iridate $Ag_3LiIr_2O_6$. *Phys. Rev. B* **2021**, *104*, L100416. [[CrossRef](#)]
23. Wang, J.; Yuan, W.; Imai, T.; Singer, P.M.; Bahrami, F.; Tafti, F. NMR investigation on the honeycomb iridate $Ag_3LiIr_2O_6$. *Phys. Rev. B* **2021**, *103*, 214405. [[CrossRef](#)]
24. Abramchuk, M.; Ozsoy-Keskinbora, C.; Krizan, J.W.; Metz, K.R.; Bell, D.C.; Tafti, F. Cu_2IrO_3 : A New Magnetically Frustrated Honeycomb Iridate. *J. Am. Chem. Soc.* **2017**, *139*, 15371–15376. [[CrossRef](#)] [[PubMed](#)]
25. Kenney, E.M.; Segre, C.U.; Lafargue-Dit-Hauret, W.; Lebedev, O.I.; Abramchuk, M.; Berlie, A.; Cottrell, S.P.; Simutis, G.; Bahrami, F.; Mordvinova, N.E.; et al. Coexistence of static and dynamic magnetism in the Kitaev spin liquid material Cu_2IrO_3 . *Phys. Rev. B* **2019**, *100*, 094418. [[CrossRef](#)]
26. Choi, Y.; Lee, C.; Lee, S.; Yoon, S.; Lee, W.J.; Park, J.; Ali, A.; Singh, Y.; Orain, J.C.; Kim, G.; et al. Exotic Low-Energy Excitations Emergent in the Random Kitaev Magnet Cu_2IrO_3 . *Phys. Rev. Lett.* **2019**, *122*, 167202. [[CrossRef](#)]
27. O'Malley, M.J.; Verweij, H.; Woodward, P.M. Structure and properties of ordered Li_2IrO_3 and Li_2PtO_3 . *J. Solid State Chem.* **2008**, *181*, 1803–1809. [[CrossRef](#)]
28. Bahrami, F.; Kenney, E.M.; Wang, C.; Berlie, A.; Lebedev, O.I.; Graf, M.J.; Tafti, F. Effect of structural disorder on the Kitaev magnet $Ag_3LiIr_2O_6$. *Phys. Rev. B* **2021**, *103*, 094427. [[CrossRef](#)]
29. Kitagawa, K.; Takayama, T.; Matsumoto, Y.; Kato, A.; Takano, R.; Kishimoto, Y.; Bette, S.; Dinnebier, R.; Jackeli, G.; Takagi, H. A spin-orbital-entangled quantum liquid on a honeycomb lattice. *Nature* **2018**, *554*, 341–345. [[CrossRef](#)]
30. Tsirlin, A.A.; Gegenwart, P. Kitaev Magnetism through the Prism of Lithium Iridate. *Phys. Status Solidi* **2021**. [[CrossRef](#)]
31. Bette, S.; Takayama, T.; Kitagawa, K.; Takano, R.; Takagi, H.; Dinnebier, R.E. Solution of the heavily stacked faulted crystal structure of the honeycomb iridate $H_3LiIr_2O_6$. *Dalton Trans.* **2017**, *46*, 15216–15227. [[CrossRef](#)] [[PubMed](#)]
32. Balzar, D. X-ray Diffraction Line Broadening: Modeling and Applications to High- T_c Superconductors. *J. Res. Natl. Inst. Stand. Technol.* **1993**, *98*, 321–353. [[CrossRef](#)] [[PubMed](#)]
33. Abramchuk, M.; Lebedev, O.I.; Hellman, O.; Bahrami, F.; Mordvinova, N.E.; Krizan, J.W.; Metz, K.R.; Broido, D.; Tafti, F. Crystal Chemistry and Phonon Heat Capacity in Quaternary Honeycomb Delafossites: $Cu[Li_{1/3}Sn_{2/3}]O_2$ and $Cu[Na_{1/3}Sn_{2/3}]O_2$. *Inorg. Chem.* **2018**, *57*, 12709–12717. [[CrossRef](#)] [[PubMed](#)]
34. Rau, J.G.; Lee, E.K.H.; Kee, H.Y. Spin-Orbit Physics Giving Rise to Novel Phases in Correlated Systems: Iridates and Related Materials. *Annu. Rev. Condens. Matter Phys.* **2016**, *7*, 195–221. [[CrossRef](#)]
35. Kim, H.S.; Kee, H.Y. Crystal structure and magnetism in α - $RuCl_3$: An ab initio study. *Phys. Rev. B* **2016**, *93*, 155143. [[CrossRef](#)]
36. Winter, S.M.; Li, Y.; Jeschke, H.O.; Valentí, R. Challenges in design of Kitaev materials: Magnetic interactions from competing energy scales. *Phys. Rev. B* **2016**, *93*, 214431. [[CrossRef](#)]
37. Rau, J.G.; Lee, E.K.H.; Kee, H.Y. Generic Spin Model for the Honeycomb Iridates beyond the Kitaev Limit. *Phys. Rev. Lett.* **2014**, *112*, 077204. [[CrossRef](#)]
38. Rusnacko, J.; Gottfryd, D.; Chaloupka, J. Kitaev-like honeycomb magnets: Global phase behavior and emergent effective models. *Phys. Rev. B* **2019**, *99*, 064425. [[CrossRef](#)]
39. Choi, S.K.; Coldea, R.; Kolmogorov, A.N.; Lancaster, T.; Mazin, I.I.; Blundell, S.J.; Radaelli, P.G.; Singh, Y.; Gegenwart, P.; Choi, K.R.; et al. Spin Waves and Revised Crystal Structure of Honeycomb Iridate Na_2IrO_3 . *Phys. Rev. Lett.* **2012**, *108*, 127204. [[CrossRef](#)]
40. Takahashi, S.K.; Wang, J.; Arsenault, A.; Imai, T.; Abramchuk, M.; Tafti, F.; Singer, P.M. Spin Excitations of a Proximate Kitaev Quantum Spin Liquid Realized in Cu_2IrO_3 . *Phys. Rev. X* **2019**, *9*, 031047. [[CrossRef](#)]

41. Knolle, J.; Moessner, R.; Perkins, N.B. Bond-Disordered Spin Liquid and the Honeycomb Iridate $\text{H}_3\text{LiIr}_2\text{O}_6$: Abundant Low-Energy Density of States from Random Majorana Hopping. *Phys. Rev. Lett.* **2019**, *122*, 047202. [[CrossRef](#)] [[PubMed](#)]
42. Kao, W.H.; Knolle, J.; Halász, G.B.; Moessner, R.; Perkins, N.B. Vacancy-Induced Low-Energy Density of States in the Kitaev Spin Liquid. *Phys. Rev. X* **2021**, *11*, 011034. [[CrossRef](#)]
43. Pal, S.; Seth, A.; Sakrikar, P.; Ali, A.; Bhattacharjee, S.; Muthu, D.V.S.; Singh, Y.; Sood, A.K. Probing signatures of fractionalization in the candidate quantum spin liquid Cu_2IrO_3 via anomalous Raman scattering. *Phys. Rev. B* **2021**, *104*, 184420. [[CrossRef](#)]
44. Frolov, S. Quantum computing's reproducibility crisis: Majorana fermions. *Nature* **2021**, *592*, 350–352. [[CrossRef](#)]
45. Field, B.; Simula, T. Introduction to topological quantum computation with non-Abelian anyons. *Quantum Sci. Technol.* **2018**, *3*, 045004. [[CrossRef](#)]
46. You, Y.Z.; Kimchi, I.; Vishwanath, A. Doping a spin-orbit Mott insulator: Topological superconductivity from the Kitaev-Heisenberg model and possible application to $\text{Na}_2/\text{Li}_2\text{IrO}_3$. *Phys. Rev. B* **2012**, *86*, 085145. [[CrossRef](#)]